E017-2595 R1

Research paper manuscript for publication consideration in
Electrochimica Acta

Effect of bromide adsorption on electrowetting of Au electrode with hexadecane

Tetsuro Morooka[a], Hironobu Tahara[b], Takamasa Sagara[b,*]

[a]*Department of Advanced Technology and Science for Sustainable Development, Graduate School of Engineering, Nagasaki University, Bunkyo 1-14, Nagasaki 852-8521, Japan*
[b]*Division of Chemistry and Materials Science, Graduate School of Engineering, Nagasaki University, Bunkyo 1-14, Nagasaki 852-8521, Japan*

Keywords:
Alkane droplet, *Au(1 1 1) electrode*, *Bromide adsorption*, *Contact angle*, *Potential-controlled shape change*

*Corresponding authors. Tel. & fax : +81-95-819-2676
E-mail address: sagara@nagasaki-u.ac.jp (T. Sagara)
http://www.cms.nagasaki-u.ac.jp/lab/douteki/jp/index.html

Summary

- Contact angle (θ) change of an *n*-hexadecane droplet was tracked in water.
- Br^- adsorption lowered the Au(1 1 1) electrode/water (S/W) interfacial tension.
- Br^- adsorption raised θ of the droplets of 1 μL and < ca. 33 pL.
- A plot of θ vs. surface charge enabled us to pinpoint Br^- desorption potential.

Abstract

Electrowetting of a Au/aqueous solution interface with hexadecane (HD) was largely affected by specific adsorption of Br^- on the Au surface. The adsorption distinctly changed the potential dependence of the contact angle (θ) of HD droplets on a Au(1 1 1) electrode surface in line with electrocapillary relationship. Measurements of θ as a macroscopic observable, being sensitive to the atomic level change of the electrode surface such as surface reconstruction and Br^- adsorption, allowed us to monitor the state of the Au/aqueous solution interface as demonstrated by pinpointing the Br^- desorption potential. The amplitude of potential-controlled reshaping of a HD 1.0 μL droplet was enhanced by specific adsorption of Br^-. The specific adsorption also affected HD microdroplets (< 50 μm diameter ≈ 33 pL volume) in the same way as 1.0 μL droplets as revealed by *in situ* electrochemical fluorescence imaging measurements. Overall, ionic adsorption provides us with opportunities of fine control of the dynamics of oil droplet in an electrode potential range narrower than 1.5 V.

1. Introduction

Control of the movement of a small liquid droplet at various spatiotemporal scales is a subject of paramount importance in interfacial chemistry, painting and coating technology, and microfluidic device technology [1]. The shape of mobile droplet is described by its contact angle (θ). Balance of interfacial tensions at the peripheral three-phase contact line of a droplet determines θ. In-depth understanding of mechanisms of the shape change and movement of a droplet on a solid substrate provides us with the basis to realize locomotion of the droplet at will. For this purpose, the use of voltage application to change the interfacial tension has advantages over other techniques for rapid regulation, repeatability, and controllability.

Electrode potential-controlled change of the interfacial tension balance for an oil droplet at an electrode/aqueous electrolyte solution interface has been extensively studied since Lippmann's demonstration of electrocapillary phenomena in the 19th-century [2]. In 1998, Welters and Fokkink achieved reversible and repeatable shape change of an aqueous electrolyte droplet in air on a thin dielectric material coated on an electrode [3]. This functional mechanism using a dielectric thin film is called "electrowetting on dielectric (EWOD)". It found applications, for instance, to a focus-changeable optical lens in air [4], although its operation needs over 30 V of applied voltage. Even on a bare metal electrode, reversible shape change of a liquid droplet has been achieved. Ivošević and Žutić demonstrated a large magnitude of shape change of *n*-hexadecane (HD) droplet of 75 μL on a Hg electrode in an aqueous electrolyte solution driven by potential dependent interfacial tension of the Hg/solution interface [5]. The shape change of the droplet placed directly on a bare metal electrode is called "electrowetting on conductor (EWOC)". The EWOC-type shape change of an insulating dielectric oil droplet placed on an electrode surface in water is in principle controlled by the interfacial tension at the solid electrode/water interface, $\gamma_{S/W}$, as far as two other interfacial tensions, $\gamma_{O/W}$ and $\gamma_{S/O}$, are potential independent, where $\gamma_{O/W}$ is the interfacial tension at the oil/water interface and $\gamma_{S/O}$ at the electrode/oil interface. Until now, various mechanisms of EWOC have been unveiled [6–13].

In this work, we use specific adsorption of bromide ion (Br^-) to change $\gamma_{S/W}$ with an aim at describing the mechanism of shape change of a HD liquid droplet in the presence of Br^- in aqueous electrolyte solution on a single crystal Au(1 1 1) electrode in *ca*. 1.5 V range of the electrode potential. Presumably, the specific adsorption directly changes the structure of the electric double layer, resulting in the emergence of a new type of potential-controlled shape change of an oil droplet. Microscopic structural changes of the electrode/solution interface caused by Br^- adsorption may reflect in the macroscopically observable θ of HD droplets through the change of the interfacial tension balance as a function of the electrode potential and Br^- concentration, c_{KBr}. In turn, obtained θ should be an essential measure to understand the adsorption of Br^- through the droplet shape. We use HD, especially of 1 μL volume, as the insulating dielectric oil phase, for which we can assume that $\gamma_{O/W}$ and $\gamma_{S/O}$ are constant in the potential range used in this work. As for Br^- adsorption, potential dependent adsorption layer structures on a Au(1 1 1) electrode have been extensively reported and reviewed [14–16].

Examination of different droplet sizes is worth to evaluate whether the scale is a significant factor of the influence of Br^- adsorption to θ or not. As an approach, we also track the potential-controlled behavior of microdroplet of HD < 50 μm diameter size, corresponding to < ca. 33 pL volume, by the use of the electrochemical fluorescence microscope in the presence of Br^-, in addition to the behavior of a 1 μL volume droplet. In previous work, we revealed the morphology of liquid HD of a less than 10000 mono-molecular layer equivalent amount on a Au(1 1 1) electrode surface [17]. HD is reversibly driven by electrode potential change so that HD forms microdroplets, the height of which is greater at more negative potentials. HD never spreads to be a continuous liquid film even around the potential of zero charge (pzc). The change of the microdroplet height due to reshaping with the electrode potential is repeatable, and the change takes place even in farther region beyond the double layer thickness. These results were obtained by the electrochemical fluorescence microscopy [17]. The fluorescence from probe molecules in the proximity of the metal surface is largely quenched depending on the probe-metal distance [18–21]. It should be emphasized that fluorescence microscopic observation enables us not only to figure out 2D

morphologies on the electrode surface in the optical microscopic scales but also to detect the movement of the probe dye molecules in the surface-normal direction in nanometer scales.

To deposit microdroplet of HD in our previous work, we used touching method [17] (see also 2.2. below). The drawback of this method includes that the precise amount of deposited HD on the electrode surface is unknown and that the measurement of θ is difficult. If a 1 μL droplet behaves the same way as a microdroplet in regard to potential dependence and if it does not fragmentate to be small droplets, we can describe the behavior authentically over the range of several μL to 33 pL quantitatively and discuss the droplet dynamics using the surface tension balance change. Therefore, it is of importance to overview experimentally these two scales of the droplet size.

2. Experimental

2.1. Materials

The reagent grade HD was obtained from TCI. Its purity was checked by UV-vis absorption and fluorescence spectra to affirm the absence of light absorbing or emitting impurity. Water was purified through a Milli-Q integral (Millipore) to a resistivity over 18 MΩ cm. Potassium perchlorate ($KClO_4$) of the highest reagent grade from Wako was recrystallized three times from water and was dried in vacuo. A fluorescence probe dye, perylene (Pr) of the highest reagent grade from Kanto Kagaku, was used as received. The fluorescence and excitation spectra of this dye are found in our previous report [17]. Ar gas was of 99.9995% purity. All other chemicals were of the highest reagent grade commercially available and were used as received.

A rod of cylindrical single crystal Au with a (1 1 1) surface base with an area of A = 0.272 cm^2 was purchased from Techno Chemics Inc. Immediately before its uses as a working electrode, the crystal was flame-annealed and quenched by water. A Ag|AgCl electrode in saturated KCl solution served as a reference electrode, and a coiled Au wire served as a

counter electrode. The quality of the Au(1 1 1) electrode was examined by comparing its cyclic voltammogram (CV) and differential capacity-potential (*C-E*) curve in 50 mM $KClO_4$ solution with those in a previous report [22].

2.2. Electrochemical measurements

A quartz electrochemical cell was boiled in a sulfuric acid + nitric acid mixture and was rinsed with a copious amount of purified water before use. The reference electrode was set in a separate compartment, which was connected to the main compartment through a liquid junction bridge. All the voltammetric and electrochemical fluorescence measurements were made by setting the Au(1 1 1) electrode in a hanging-meniscus (H-M) configuration to the electrolyte solution under a wetted Ar atmosphere in a Faraday cage at room temperature (22±2°C). We used 50 mM $KClO_4$ aqueous solution as the base solution.

HD was deposited on the Au(1 1 1) electrode surface using one of the following two procedures.

Procedure A: The Au(1 1 1) electrode was flame-annealed and quenched by water. This anneal/quench cycle was repeated several times. The electrode after final annealing was cooled to room temperature in the Ar gas flow. The cooled Au(1 1 1) electrode surface was touched to the neat HD liquid/air interface for a period of 10 s, and then dipped in hexane for 10 s. Subsequently, the electrode covered with HD + hexane was placed in the Ar gas flow for 10 min to completely evaporate hexane. When necessary, incorporation of a probe dye was made by touching the HD covered electrode surface to 2.0 μM Pr/hexane solution for a period of 10 s. The electrode was then touched to hexane for 10 s and placed in the Ar gas flow for 10 min to evaporate hexane. Note that this procedure A is almost the same as Procedure 1 (touching method) in our previous report [17].

Procedure B: The Au(1 1 1) electrode was flame-annealed and then cooled in Ar gas down to room temperature. Immediately after being cooled, a hanging droplet of neat HD (1.0 μL) was placed near the center of the circular Au(1 1 1) electrode surface in air using a

micro-syringe. The electrode was horizontally touched to the surface of the solution in the quartz cell from the Ar gas phase at open-circuit and set in a H-M configuration by subsequent vertical lifting so that only the (1 1 1) surface base was in contact with the solution. When adding a probe dye, 2.0 μM Pr was dissolved in HD before forming the droplet. Note that this procedure B is almost the same as Procedure 3 in our previous report [17].

Electrode potentials were controlled by a potentiostat (HUSO Electro Chemical System, HECS 9002) connected with a function generator. *C*-*E* curves were obtained from the ac voltammograms assuming an equivalent series circuit of a capacitance of *C* and a resistance; *C* was equated to $[-2\pi f\,\mathrm{Im}(Z)]^{-1}$, where *f* is the ac frequency of the ac potential modulation and Im(*Z*) is the imaginary part of the ac impedance. For ac measurements, a lock-in amplifier (EG&G Instruments, model 7265) was employed, and the *C*-*E* curves were obtained using an ac modulation at $f = 14$ Hz with an amplitude of 5 mV_{rms}.

2.3. Electrochemical fluorescence microscopic measurements

An electrochemical fluorescence microscope was set as shown in our previous report [17]. The base microscope (Nikon eclipse TE300) was equipped with a 100 W Hg lamp and a CCD camera (JAI, 755 Intelligent ICCD Camera). The objective lens was ×10 or ×40 Plan Fluor (Nikon). A Au(1 1 1) electrode with HD on its surface was set in a H-M configuration at a 50 mM $KClO_4$ solution surface under an Ar atmosphere in a home-designed quartz cell equipped with a bottom optical window made of a glass bottom dish (Matsunami, D111300). Fluorescence images were captured by the CCD camera at 30 frame s^{-1}.

For the measurements of θ of a HD 1.0 μL droplet, we used a digital microscope (J500-extreme) to capture an image of the droplet on the electrode in the cell. The obtained image was distorted by the curvature of the vertically-cylindrical electrochemical cell glass wall. The captured images were corrected in reference to a standard image of a perfect-sphere

model ball lens (TECHSPEC N-BK7) of nearly the same size of the droplet to evaluate θ; the correction was to compress the horizontal length by ×0.78.

The gravity negligibly affects the shape of a droplet smaller than the capillary length expressed as $(\gamma_{O/W}/\rho g)^{1/2}$ [23]; the capillary length of HD in water is 2.6 mm using the interfacial tension of oil-water interface, $\gamma_{O/W} = 53$ mN m^{-1} [24], the density of the oil, 0.7734 g cm^{-3} [25], and the gravitational acceleration, $g = 9.8$ m s^{-2}. The droplet diameter in this study was always smaller than 1.8 mm, being smaller than the capillary length.

3. Results and Discussion

3.1. Voltammograms with HD 1 μL droplet

Fig. 1.

We first use the results of voltammetric measurements shown in Fig. 1 to describe a Au(1 1 1) electrode with a HD 1.0 μL droplet (Procedure B) in 50 mM $KClO_4$ aqueous solution. CV and *C-E* curve (Figs. 1a and 1b) were measured by setting an initial potential at 0.4 V, whereas θ was tracked by scanning 0.0 V → –0.7 V → 0.6 V → 0.0 V (Fig. 1c). Fig. 1d shows the fractional coverage by a HD 1 μL droplet on Au(1 1 1) electrode as a function of the electrode potential calculated from Fig. 1c using the photographically measured circular droplet diameter, *a*, and the diameter, *b*, of the circular Au(1 1 1) surface. The fractional coverage of surface area by the HD 1 μL droplet was calculated as a^2/b^2. The fractional coverage of the electrically insulating HD 1.0 μL droplet is less than 7% of the total electrode area (Fig. 1d) and constant at more positive potentials than –0.2 V. This fact ensures that the responses positive to –0.2 V in Figs. 1a and 1b exclusively originated from the Au surface uncovered with a HD 1.0 μL droplet. Within the potential range of the θ change from –0.7 V to –0.2 V, the current and capacitance with a HD 1 μL droplet are slightly smaller than the values of a bare electrode. Change of the contact area with potential was 2% (Fig. 1d). The

corresponding decrease of voltammetric current is estimated to be 0.1 μA and that of the capacitance value to be 0.02 μF cm^{-2}. These decreases of responses are so small as to be obviously seen in CV and *C-E* curve (Fig. 1a and 1b). The current and capacitance hysteresis corresponding to the contact area change is in fact not observed in CV and *C-E* curve. We should keep in mind the possible existence of HD microdroplets invisible by naked eyes in the area of the Au(1 1 1) surface uncovered with a HD 1.0 μL droplet. As we described in our previous report [17], the microdroplets are usually smaller than 50 μm in diameter if any.

A couple of peaks around 0.03 V in the CV (Fig. 1a) as well as a broad peak and a change of the capacitance level in the range of –0.10 V to 0.20 V in the *C-E* curve (Fig. 1b) are observed for the Au(1 1 1) electrode with a deposited HD 1.0 μL droplet. In these potential regions, however, the 1.0 μL droplet does not change its coverage of the electrode surface (Figs. 1c and 1d). These observations lead to a conclusion that, other than the 1.0 μL droplet, HD really stays put as microdroplets in the area of Au(1 1 1) surface uncovered with a HD 1.0 μL droplet, and the microdroplets give rise to voltammetric responses in Figs. 1a and 1b. The responses are in line with those of a HD-covered electrode prepared by the procedure A, as we reported previously [17]; a HD-covered electrode prepared by the procedure A also exhibits a couple of CV peaks around 0.05 V and the low capacitance range from 0.10 V to 0.40 V in the *C-E* curve.

Taken together, the voltammetric responses in Figs. 1a and 1b are wholly ascribable to the processes at the Au surface uncovered with a HD 1.0 μL droplet. HD microdroplets on the electrode dominate completely the electrochemical responses in the CV and *C-E* curve (Fig.1a and 1b).

Note a significant difference of the potential dependence between a HD 1.0 μL droplet and microdroplets; Fig. 1c showed that the θ of the 1.0 μL droplet commences to increase at –0.5 V in the negative potential scan, whereas the microdroplet commences to change its shape around 0.1 V as seen in Figs. 1a and 1b and as observed in our previous work [17] also by fluorescence microscopy. This difference indicates that more negative potential is needed for a larger droplet to start the decrease of θ. This fact demonstrates the need of experiments with different droplet sizes to explore the potential-dependent behavior of HD droplets.

Fig. 2.

A fluorescence image in Fig. 2a shows the edge of a HD 1.0 μL droplet with a Pr captured on the left-hand side of the photo at −0.20 V. The other area does not show detectable fluorescence. This image, however, does not necessarily mean non-existence of HD there; it is likely that small droplets exist with low enough heights for the fluorescence of the dye molecules in HD to be quenched [17]. Fig. 2b is the photo taken when the electrode potential reached −0.70 V. We find a number of fluorescent spots depicting many HD microdroplets with diameters far smaller than 50 μm. Their heights are enough to get out of the range of the metal quenching of fluorescence. These microdroplets look the same as those observed when HD was deposited at the electrode surface using the touching method [17]. Importantly, these fluorescent spots at −0.70 V are observed only in the Au/solution interface portion that has never been swept by the HD 1.0 μL droplet under potential control. These microdroplets hardly coalesce with the HD 1.0 μL droplet and never affect the potential-dependent shape change of the 1.0 μL droplet.

For a Au(1 1 1) electrode subjected to the touching method (Procedure A), the CV and *C-E* curve (Fig. 2 in [17]) were almost same as Figs. 1a and 1b. This fact supports that the response in Fig. 1 originates from the microdroplets. When a HD 1.0 μL droplet was deposited onto a dry Au(1 1 1) surface, the droplet in air spread much more widely than the droplet in water. Whenever a Au electrode with a HD droplet was dipped in the aqueous electrolyte solution, the droplet retracted on the electrode surface to increase θ. Most likely, this shape change process left many microdroplets as footprints at the Au/solution interface. We never observed these microdroplets, if a 1.0 μL HD droplet was put on the Au electrode surface in the electrolyte solution.

3.2. Contact angle as a function of surface charge density

Fig. 1c shows θ values as measured by scanning the electrode potential; θ has greater values at negative potentials than the constant value at positive potentials. This indicates a decrease of $\gamma_{S/W}$ at the negative potentials. The θ–E curve, however, exhibits significant hysteresis depending on the sweep direction. The hysteresis, the difference of θ at the same potential coming from different sweep direction, may be caused by two reasons: (1) the potential cycling generates non-equilibrium state so that the state at a given potential reached from more positive potentials is different from that reached from more negative potentials, (2) regardless of whether equilibrium state is reached or not, difference between an advancing and a receding θ causes the difference. Several methods to suppress the reason (2) have been known including, for example, a method to give potential pulses for relaxation [7]. In this work, we conducted the potential step measurements of θ as an approach to find reliable values at near equilibrium state at each potential.

Fig. 3.

The obtained $\cos\theta$–E curve for the HD 1.0 μL droplet on a Au(1 1 1) electrode by potential step is shown in Fig. 3a. The initial potential (E_i) was −0.60 V to obtain the data points of positive-going final potentials (E_f) (open circles), whereas E_i = 0.40 V was set to obtain the points for negative-going (close circles). After the droplet shape became steady, θ measurements were undertaken. Although the decrease of θ commences at −0.05 V, a more negative potential than in Fig. 1c, large hysteresis of θ is still observed especially in the negative potential region. Also at positive potentials, hysteresis newly emerges.

As far as we regard θ as a function of electrode potential, the hysteresis cannot be suppressed. An essential variable describing the electrode/solution interface is the surface charge density, σ_M [26]. We, therefore, represent θ as a function of σ_M. To obtain the $\cos\theta$–σ_M curve, the use of σ_M measured for the Au electrode with a HD 1.0 μL droplet is inappropriate, because the coexistent microdroplets (Fig. 2b) affect σ_M. Instead, we use a σ_M–E curve of a bare Au(1 1 1) electrode in the absence of HD to obtain the θ–σ_M curve.

We observed no HD microdroplet in the area swept by the movement of a HD 1.0 μL droplet by the fluorescence measurement (Fig. 2). The electrode area in the proximity to the HD 1.0 μL droplet is of bare Au (at least free of liquid HD). The θ of a HD droplet at an electrode/water interface is determined by the interfacial tension balance at a three phase contact line, whereas the angle is not affected by the surface condition far away from the three phase contact line. The electrode surface at and out of the three phase contact line is equivalent to the bare electrode. Therefore, we use the σ_M of the bare electrode to evaluate the electrode surface condition.

The σ_M–E curve in Fig. 3b was obtained in the absence of HD using the same potential control protocol as that used to obtain Fig. 3a. The σ_M-E curves were obtained by a potential step train chronoamperometry followed by current integration using the well-established protocol [27]. The σ_M–E curve of the electrode used in the present work clearly depends on the potential step direction in the potential region between –0.60 V and 0.15 V. When stepping the potential from –0.60 V to the final potentials in between –0.60 V and 0.40 V, the final state is the reconstructed surface; when stepping the potential negatively from 0.40 V, the final state is the unreconstructed surface [28]. Because of the slow kinetics of the surface reconstruction, the surface structures at the final potentials assume a metastable state in the range between –0.60 V and 0.40 V [28]. This inevitably produces the step direction dependent σ_M values.

The interfacial tension balance at the foot edge of an oil droplet on the substrate in water is written by the Young's equation:

$$\gamma_{O/W} \cos\theta = \gamma_{S/W} + \gamma_{S/O} \quad (1)$$

On an electrode surface, $\gamma_{S/W}$ is described by the electrocapillary equation:

$$-d\gamma_{S/W} = \sigma_M dE + \Gamma_{(Br^-)} RT d\ln c_{KBr} \quad (2)$$

where E is the electrode potential in reference to the pzc, $\Gamma_{(Br^-)}$ is the Gibbs surface excess of Br^-. The value of σ_M at a given potential is sensitive to the surface condition such as surface reconstruction structure, presence and structural changes of an organic adlayer, and specifically adsorptive anions if any. Therefore, the use of $\cos\theta$–σ_M curve is well-suited to describe the potential-controlled shape change of the oil droplet on a metal electrode surface.

The data set of the θ as a function of E, $\theta(E)$ in Fig. 3a, was converted to a new set of $\theta(\sigma_M)$ by substitution of E for σ_M using the σ_M–E curves (Fig. 3b). We have two sets of $\theta(E)$ used to obtain a negative-going set of $\theta(\sigma_M)$ with $E_i = 0.40$ V and a positive-going set of $\theta(\sigma_M)$ with $E_i = -0.60$ V, and these are plotted as $\cos[\theta(\sigma_M)]$ in Fig. 3c. In sharp contrast to Figs. 1c and 3a, hysteresis in negative σ_M region is largely suppressed. Almost overlapped $\cos\theta$ is obtained by potential step measurements in negative and positive directions in the σ_M range from -30 μC cm^{-2} to -15 μC cm^{-2}. These results reveal that θ is uniquely determined by σ_M rather than E.

In conclusion, θ is sensitive to whether the electrode surface is reconstructed or unreconstructed, and σ_M is more essential variable to specifically describe θ. The hysteresis in θ–E curve (Fig. 1c) obtained by potential sweep method contains partly the difference between the advancing and receding angles, because it is relatively greater than the hysteresis in Fig. 3a.

3.3. Effect of Br^- adsorption upon the potential-controlled shape change of HD droplet

Fig. 4.

Fig. 4 shows a CV in 2.0 mM KBr + 50 mM $KClO_4$ aqueous solution for a Au(1 1 1) electrode with HD deposited by the touching method (Procedure A). The sharp positive current peak at -0.03 V represents the lift of the (1×23) reconstruction of the Au(1 1 1) surface in the presence of Br^- [29]. The broad positive hump peaked around 0.15 V corresponds to the formation of a disordered Br^- adlayer. The CV displays also a small peak

pair at 0.53 V caused by the phase transition between the disordered and ordered ($\sqrt{3} \times \sqrt{7}$) Br^- adlayer [30]. The asymmetry of CV between positive and negative going potential sweeps indicates slow kinetics of lift and restoration of the reconstructed (1×23) structure of the Au surface [31]. The CV curve is almost the same as CV for a bare Au(1 1 1) electrode in 2 mM KBr aqueous solution in spite of the existence of microdroplets. Specific adsorption of Br^- is not strongly blocked by HD microdroplets. Most likely, the microdroplets are repelled by Br^- adsorption layer and thus squeezed at their foot regions, giving rise to the CV response dominated by adsorption/desorption of Br^-. Such a squeeze should be experimentally observed for both microdroplets and a 1.0 μL droplet, as Fig. 7 later demonstrates (vide infra).

Fig. 5.

Fig. 5 shows a plot of $\cos\theta$ versus σ_M for a HD 1.0 μL droplet on Au(1 1 1) electrode surface in 2.0 mM KBr + 50 mM $KClO_4$ aqueous solution. Potential step procedures used to obtain the plot are given in the figure caption. In Eq. (1), we can assume that $\gamma_{O/W}$ (53 mN m^{-1}) and $\gamma_{S/O}$ are constant. Therefore, using positive constants p and q, we can write

$$\cos\theta = p\,\gamma_{S/W}(\sigma_M) + q \qquad (3)$$

Eq. (3) demonstrates that the experimental $\cos\theta$–σ_M plot should have the same curve shape as a $\gamma_{S/W}$–σ_M plot, the electrocapillary curve, although $\gamma_{S/W}$ is not a directly measurable quantity for a solid electrode. The plot in Fig. 5 is, therefore, equivalent to a representation of a part of the electrocapillary curve in the presence of Br^-. The position of $\sigma_M = 0$ is the pzc in the absence of Br^- but not in the presence of it. The change of one unit of the $\cos\theta$ scale (ordinate of the figure) corresponds to a $\gamma_{S/W}$ change of 53 mN m^{-1}.

The specific adsorption of Br^- increases the value of σ_M and lowers the $\gamma_{S/W}$, resulting in the retraction of the HD droplet. In both positive and negative-going processes, θ is σ_M dependent between 20 μC cm^{-2} and 50 μC cm^{-2}. In the region from −10 μC cm^{-2} to 20 μC cm^{-2}, the $\cos\theta$–σ_M curve shows a plateau. In the *absence* of KBr (Fig. 3c), we have

also found a plateau region at a level of $\cos\theta = 0.82 \pm 0.12$ in the range of $\sigma_M > -12$ μC cm^{-2}. In KBr solution, a much lower plateau level of $\cos\theta = 0.19$ is observed (Fig. 5), and the plateau range is included in the potential range of Br^- adsorption. Obviously, the presence of an adlayer of Br^- largely truncates the electrocapillary curve. The specific adsorption of Br^- increases the value of σ_M and lowers the $\gamma_{S/W}$ in the region of 20 μC cm^{-2} < σ_M < 50 μC cm^{-2}, resulting in the change of $\cos\theta$ of the HD droplet in both positive and negative-going processes. The specific adsorption Br^- occurs in the region 20 μC cm^{-2} < σ_M < 50 μC cm^{-2} and HD droplet is squeezed at its foot region because of the increasing surface pressure of the adsorption layer of Br^-. In the region σ_M > 50 μC cm^{-2}, the second plateau emerges. Potential scanning in this largely positive region was avoided in this work not to reach Au surface oxidation, which may result in complexity in the adhesion of the droplet.

The σ_M obtained in the negative-going process have an inflection point around −20 μC cm^{-2} as a diamond marks in Fig. 5. In the positive-going process, corresponding inflection is not found. The curve positive to the inflection point in the negative-going process overlaps with the curve of the positive-going process in KBr solution, whereas the curve negative to the inflection point in the negative-going process overlaps with the curve obtained in $KClO_4$ solution without KBr. Before the inflection point is reached in the negative-going process, adsorbed Br^- lowers θ from that in the absence of adsorbed species. The inflection point, therefore, pinpoints the Br^- desorption potential (around −0.45 V vs $E_{Ag/AgCl\ sat'd\ KCl}$) in 2.0 mM KBr solution.

3.4. Droplet reshaping by potential sweep in the presence of Br^-

Fig. 6.

Fig. 6 sheds a light on the θ–E curves obtained by the potential sweep measurements. An addition of 5.0 mM KBr changes the θ–E curve; sizable increase of the amplitude of

potential-controlled droplet shape change emerges. A sharp rise of θ from 0.05 V to 0.30 V corresponds to a steep increase of the specific adsorption amount of Br^-.

In Fig. 6, representative σ_M values are noted for reference. In the absence of KBr, the positive potential sweep reaches the plateau region of θ at –0.20 V, at which σ_M value is –26 μC cm^{-2}. The plateau region extends to σ_M = 32 μC cm^{-2}. In the presence of 5.0 mM KBr, the positive potential sweep terminates a lower plateau at $\sigma_M > 32$ μC cm^{-2} and initiates the higher second plateau of $\theta = 111°$, which extends to $\sigma_M > 88$ μC cm^{-2}. The droplet shape is determined by σ_M through $\gamma_{S/W}$ also in the potential sweep method.

Apparent hysteresis originated from the direction of the potential sweep is found in the regions of $\sigma_M < -17$ μC cm^{-2} (with KBr) and $\sigma_M < -26$ μC cm^{-2} (without KBr). These close values of σ_M also indicate that σ_M is the essential variable determining θ through the change of $\gamma_{S/W}$. The curve shapes with hysteresis in these two conditions are nearly the same, because Br^- adsorption amount is small or zero in these negative potential regions. The difference of the θ value at the edge of these potential regions may cause the different θ value levels at more negative potentials while giving a similar curve shape. In 5 mM KBr solution, another hysteresis of θ–E curve was observed in the range from –0.20 V to 0.30 V, which corresponds to the potential region in which the direction of potential sweep determines adsorption-desorption of Br^-.

To sum up, the θ of a HD 1.0 μL droplet on an electrode surface is increased by the specific adsorption layer of Br^-. Clearly, a macroscopically observable value, θ, is determined by the atomic level changes on the electrode surface, demonstrating a typical case that nano-level phenomena result in the change of a macroscopic state observable by the naked eyes.

3.5. Scaling of droplet reshaping in the presence of Br^-

Fig. 7

It is worthwhile to see whether KBr concentration affects the microdroplets and the 1.0 μL droplets in the same way or not. The surface excess of Br^- increases with increasing c_{KBr} [15]. The increase of θ of a HD droplet is therefore predicted.

First, we measured the potential-controlled change of θ of the 1.0 μL droplet in 50 mM and 500 mM KBr solutions (Fig. 7a and 7b). The obtained θ values obviously depend on the c_{KBr}. The θ values both in the Br^- specific adsorption potential region from 0.0 V to 0.6 V and in negative potential region from –0.7 V to 0.0 V are greater in 500 mM than in KBr 50 mM solution. In reference to Eq. (2), the interfacial tension $\gamma_{S/W}$ decreases with increasing c_{KBr}. The higher surface pressure with more Br^- adsorption amounts results in the greater θ of a HD 1.0 μL droplet.

Second, the height of microdroplets prepared by touching method was monitored using *in situ* fluorescence microscope in 50 mM and 500 mM KBr solutions (Figs. 7c and 7d). The deposited HD by procedure A (touching method) contained Pr as a fluorescence probe. Both the fluorescence images and fluorescence intensity curves were obtained in the course of cyclic potential sweep at $v = 5$ mV s^{-1}. The integrated fluorescence intensity values, I_{FL}, obtained from the fluorescence image were plotted as a function of the electrode potential. In the microscope image of Fig. 7c, the largest bright spot has a diameter slightly over 50 μm while such a large droplet has been rarely found. This, however, does not largely affect the I_{FL}–E plot. The increment of the I_{FL} in 0.0 V – 0.4 V range, the Br^- specific adsorption potential region, is steeper in 500 mM KBr than in 50 mM KBr. The I_{FL} at 0.4 V in 500 mM KBr solution is greater than that in KBr 50 mM solution. The I_{FL} at specific adsorption region in 500 mM KBr is almost equal to that at negative potential region (Fig. 7d). Such an increment at positive potentials has never been observed in the absence of KBr in $KClO_4$ solution [17], revealing that adsorption of Br^- increases the I_{FL}. In the fluorescence microscopic measurements, the I_{FL} depends on the distance between the fluorophore and a metal electrode surface in the range up to 50 nm and farther because of the metal quenching [18,19]. The differences in the I_{FL} indicate that the heights of the HD microdroplets are in an order of 500 mM KBr > 50 mM KBr > without KBr (50 mM $KClO_4$). Even though the cyclic potential sweep was repeated, collision-coalescence or separation of the fluorescent

microdroplets was never observed. Therefore, we can conclude that the microdroplets prepared by the touching method also show greater θ at positive potentials at higher c_{KBr}. Specific adsorption of Br^- affects microdroplets to change the interfacial tension balance in the same manner as 1.0 μL droplets.

Taken together, specific adsorption of Br^- affects the droplet shape in the same way regardless the size of the droplet. *In situ* fluorescence measurements have enabled us to reveal a greater height of the microscopic droplets at 500 mM Br^- concentration than at 50 mM in the potential region of Br^- specific adsorption. The effect of Br^- adsorption at the Au/aqueous solution interface surrounding the droplets upon the potential-controlled droplet shape change works in the same way for the 1.0 μL droplet and microdroplets.

4. Conclusions

We found that Br^- adsorption at a S/W interface effects the profound variation of potential-controlled shape change of HD droplets on a Au(1 1 1) electrode surface. For both HD 1.0 μL droplet and microdroplets, the specific adsorption of Br^- affects potential-driven morphological change of the droplets. A clear hysteresis of θ of a HD droplet was observed between positive and negative potential sweeps. The hysteresis was almost suppressed by representing $\cos\theta$ as a function of σ_M obtained by the potential step measurements. We concluded that θ is determined essentially by σ_M, whereas the hysteresis in θ–E curve originates from the history-dependent state of the Au electrode surface and also partly from the difference between advancing contact angle and receding one. Surface condition of the metal electrode, reflecting in σ_M, is directly changed by specific adsorption of Br^-, resulting in the decrease in the S/W interfacial tension. The $\cos\theta$–σ_M plot enabled us to pinpoint the desorption potential of Br^-, indicating that the measurement for θ of the droplet is as the same as monitoring the S/W interface. Adsorption of Br^- induces the droplet repelling of the Au surface at specific adsorption potentials. The potential-controlled shape change was amplified by specific adsorption of Br^-.

The behavior of microdroplets of < 50 μm size is in line with that of a macroscopic droplet being affected by specific adsorption of Br^- as tracked by *in situ* fluorescence measurements. In addition, in the absence of strongly adsorptive anion such as Br^-, the need of careful interpretation of voltammetric data should be pointed out when microdroplets coexist with a large droplet; the voltammogram may be dominated by the microdroplets and the θ increase of the large droplet takes place slightly more negative potentials than the height change of the microdroplet.

Acknowledgements

The authors acknowledge with appreciation Dr. Takanori Yazawa, Nagasaki University for technical advice for the correction of droplet images. This work was supported by a Grant-in-Aid (to TS) for Scientific Research on Innovative Area "Molecular Robotics" (No. 24104004) of The Ministry of Education, Culture, Sports, Science, and Technology, Japan.

References

[1] O. D. Velev, B. G. Prevo, K. H. Bhatt, On-chip manipulation of free droplets, Nature 426 (2003) 515.

[2] G. Lippmann, Relations entre les phénomènes électriques et capillaries, Ann. Chim. Phys. 5 (1875) 494 (Translation in English: in F. Mugele, J. -C. Baret, Elecctrowetting: from basics to applications, J. Phys.: Condens. Matter 17 (2005) R705).

[3] W. J. J. Welters, L. G. J. Fokkink, Fast electrically switchable capillary effects, Langmuir 14 (1998) 1535.

[4] Y.-P. Zhao, Y. Wang, Fundamentals and applications of electrowetting: A critical review, Rev. Adhesion Adhesives 1 (2013) 114.

[5] N. Ivošević, V. Žutić, Spreading and detachment of organic droplets at an electrified interface, Langmuir 14 (1998) 231.

[6] C. B. Gorman, H. A. Biebuyck, G. M. Whitesides, Control of the shape of liquid lenses on a modified gold surface using an applied electrical potential across a self-assembled monolayer, Langmuir 11 (1995) 2242.

[7] A. A. Kornyshev, A. R. Kucernak, M. Marinescu, C. W. Monroe, A. E. S. Sleightholme, M. Urbakh, Ultra-low-voltage electrowetting, J. Phys. Chem. C 114 (2010) 14885.

[8] B. C. Gallardo, V. K. Gupta, F. D. Eagerton, L. I. Jong, V. S. Craig, R. R. Shah, N. L. Abbott, Electrochemical principles for active control of liquids on submillimeter scales, Science 283 (1999) 57.

[9] T. Nagai, S. Nakanishi, Y. Nakato, Water molecules adsorbed at electrode surface determine the macroscopic contact angles, ChemPhysChem 8 (2007) 1016.

[10] G. Zhang, M. Walker, P. R. Unwin, Low-voltage voltammetric electrowetting of graphite surfaces by ion intercalation/deintercalation, Langmuir 32 (2016) 7476.

[11] D. J. Lomax, P. Kant, A. T. Williams, H. V. Patten, Y. Zou, A. Juel, R. A. W. Dryfe, Ultra-low voltage electrowetting using graphite surfaces, Soft Matter 12 (2016) 8798.

[12] S. F. L. Mertens, A. Hemmi, S. Muff, O. Grönig, S. De Feyter, J. Osterwalder, T. Greber, Switching stiction and adhesion of a liquid on a solid, Nature 534 (2016) 676.

[13] Y. Mukouyama, T. Shiono, Spontaneous motion of nitorobenzene droplet on Au electrode during Sn electrodeposition, J. Electrochem. Soc. 163 (2016) H36.

[14] O. M. Magnussen, Ordered anion adlayers on metal electrode surfaces, Chem. Rev. 102 (2002) 679.

[15] J. Lipkowski, Z. Shi, A. Chen, B. Pettinger, C. Bilger, Ionic adsorption at the Au(1 1 1) electrode, Electrochim. Acta 43 (1998) 2875.

[16] Z. Shi, J. Lipkowski, S. Mirwald, B. Pettinger, Electrochemical and second harmonic generation study of bromide adsorption at the Au(1 1 1) electrode surface, J. Chem. Soc., Faraday Trans. 92 (1996) 3737.

[17] T. Morooka, S. Murakawa, A. Konomi, D. Goto, T. Sagara, Potential-dependent morphological change of n-hexadecane small droplets on a Au(1 1 1) electrode in aqueous

solution: A voltammetric and electrochemical fluorescence microscopic study, J. Electroanal. Chem. 779 (2016) 25.

[18] D. Bizzotto, J. L. Shepherd, Epi-fluorescence microscopy studies of potential controlled changes in adsorbed thin organic films at electrode surfaces in: R. C. Alkire, D. K. Kolb, J. Lipkowski, P. N. Ross (Eds.), Advances in Electrochemical Science and Engineering: Diffraction and Spectroscopic Methods in Electrochemistry, Vol. 9, Ch. 3, Weinheim, Wiley-VCH Verlag, 2006, p. 97.

[19] D. Bizzotto, J. Lipkowski, Electrochemical and spectroscopic studies of the mechanism of monolayer and multilayer adsorption of an insoluble surfactant at the Au(111)|electrolyte interface, J. Electroanal. Chem. 409 (1996) 33.

[20] R. R. Chance, A. Prock, R. Silbey, Molecular fluorescence and energy transfer near interfaces, Adv. Chem. Phys. 37 (1978) 1.

[21] Z.-J. Zhang, A. L. Verma, N. Tamai, K. Nakashima, M. Yoneyama, K. Iriyama, Y. Ozaki, Excitation energy transfer in Langmuir–Blodgett films of 5-(4-N-octadecylpyridyl)-10,15,20-tri-p-tolylporphyrin on gold-evaporated glass substrates studied by time resolved fluorescence spectroscopy, Thin Solid Films 333 (1998) 1.

[22] A. Hamelin, Cyclic voltammetry at gold single-crystal surfaces. Part 1. Behaviour at low-index faces, J. Electroanal. Chem. 407 (1996) 1.

[23] P. G. de Gennes, Wetting: statics and dynamics, Review of Modern Physics 57 (1985) 827.

[24] R. E. Johnson Jr., R. H. Dettre, The wettability of low-energy liquid surfaces, J. Colloid Interface Sci. 21 (1996) 610.

[25] T. Sakai, K. Kamogawa, K. Nishiyama, H. Sakai, M. Abe, Molecular diffusion of oil/water emulsions in surfactant-free conditions, Langmuir 18 (2002) 1985.

[26] C. Korzeniewski, V. Climent, J. M. Feliu, Electrochemistry at platinum single crystal electrodes, in: A. J. Bard, C. Zoski (Eds.), Electroanalytical chemistry: a series of advances, Vol. 24, Ch. 2 CRC Press, 2011, p. 75.

[27] J. Lipkowski, L. Stolberg, Molecular adsorption at gold and silver electrodes, Chap. 4, in: J. Lipkowski, P.N. Ross (Eds.), Adsorption of Molecules at Metal Electrodes, VCH, N.Y. 1992, pp. 171–238.

[28] S. Wu, J. Lipkowski, O. M. Magnussen, B. M. Ocko, Th. Wandlowski, The driving force for $(p \times \sqrt{3}) \leftrightarrow (1 \times 1)$ phase transition of Au(111) in the presence of organic adsorption: a combined chronocoulometric and surface X-ray scattering study, J. Electoanal. Chem. 446 (1998) 67.

[29] B. Pettinger, J. Lipkowski, S. Mirwald, In situ SHG studies of adsorption induced surface reconstruction of Au(1 1 1) electrodes, Electrochim. Acta 40 (1995) 133.

[30] O. M. Magnussen, B. M. Ocko, J. X. Wang, R. R. Adzic, In-situ X-ray diffraction and STM studies of bromide adsorptin on Au(1 1 1) electrodes, J. Phys. Chem. 100 (1996) 5500.

[31] D. M. Kolb, Reconstruction phenomena at metal-electrolyte interfaces, Prog. Surf, Sci. 51 (1996) 109.

Figure Captions

Fig. 1. Collection of voltammetric data in 50 mM $KClO_4$ aqueous solution for a Au(1 1 1) electrode with a HD 1.0 μL droplet using Procedure B: (a) CV at $v = 20$ mV s^{-1}, (b) *C*-*E* curve at $v = 5$ mV s^{-1}, (c) θ obtained by potential sweep method at $v = 10$ mV s^{-1}, (d) fractional coverage of the electrode surface by the HD 1.0 μL droplet calculated from (c) using the photographically measured droplet diameter. The gray lines in (a) and (b) are the data for a bare Au(1 1 1) electrode without HD.

Fig. 2. Fluorescence microscopic images with ×40 objective lens obtained in the course of potential sweep at $v = 5$ mV s^{-1} in the presence of a Pr-contained HD droplet on a Au(1 1 1) electrode surface using Procedure B at −0.20 V (a) and −0.70 V (b). The excitation wavelength ranged from 355 nm to 375 nm. The detection wavelength ranged from 395 nm to 700 nm.

Fig. 3. (a) $\cos\theta$–*E* curve obtained by potential step for a HD 1.0 μL droplet on a Au(1 1 1) electrode using Procedure B. (b) σ_M–*E* curves obtained by a potential step train coulometry for a bare Au(1 1 1) electrode in contact with 50 mM $KClO_4$ solution. For both (a) and (b), the initial potential, E_i, which is the base potential for the step train, was −0.60 V for the positive-going steps (opened circles), whereas $E_i = 0.40$ V for the negative-going steps (closed circles). (c) $\cos\theta$–σ_M curve obtained by combined use of $\cos\theta$–*E* (a) and σ_M–*E* (b) curves.

Fig. 4. CV in 2.0 mM KBr + 50 mM $KClO_4$ aqueous solution at $v = 50$ mV s^{-1} for a Au(1 1 1) electrode with HD prepared by the touching method (Procedure A).

Fig. 5. $\cos\theta$–σ_M curve for Au(1 1 1) electrode using Procedure B in contact with 2.0 mM KBr + 50 mM $KClO_4$ solution obtained by the combined use of σ_M–*E* and $\cos\theta$–*E* curves obtained by potential step measurements. Note that σ_M was measured in the absence of HD. The initial potential, E_i, which is the base potential for the step train, was −0.60 V for the

steps to positive-going process (open circles), whereas $E_i = 0.60$ V for the steps to negative-going process (close circles). A diamond mark pointed the inflection in the negative-going process. Gray data points represent $\cos\theta$–σ_M curve of a Au(1 1 1) electrode without KBr for the negative-going process.

Fig. 6. θ–E curves obtained by potential sweep at $v = 10$ mV s^{-1} for a HD 1.0 μL droplet on a Au(1 1 1) electrode surface using Procedure B in 5.0 mM KBr + 50 mM $KClO_4$ aqueous solution (red squares) and in 50 mM $KClO_4$ aqueous solution (blue squares). Added were σ_M values obtained in the absence of HD by positive-going potential step coulometry in 5.0 mM KBr + 50 mM $KClO_4$ (red arrow indications) or 50 mM $KClO_4$ (blue arrow indications).

Fig. 7. Upper part, θ–E curves with corrected typical photo images obtained by potential sweep at $v = 10$ mV s^{-1} for a HD 1.0 μL droplet on a Au(1 1 1) electrode surface using Procedure B in (a) 50 mM KBr aqueous solution, (b) 500 mM KBr aqueous solution.

Lower part; integrated fluorescence intensity (I_{FL})−potential (E) curves for HD with Pr prepared by the touching method (Procedure A) on a Au(1 1 1) electrode surface obtained in (c) 50 mM KBr aqueous solution, (d) 500 mM KBr aqueous solution. I_{FL} was obtained by integrating one screen shot of the entire fluorescence microscopic images (shown at the upper side of each plot) obtained at $v = 5$ mV s^{-1} with ×40 objective lens.

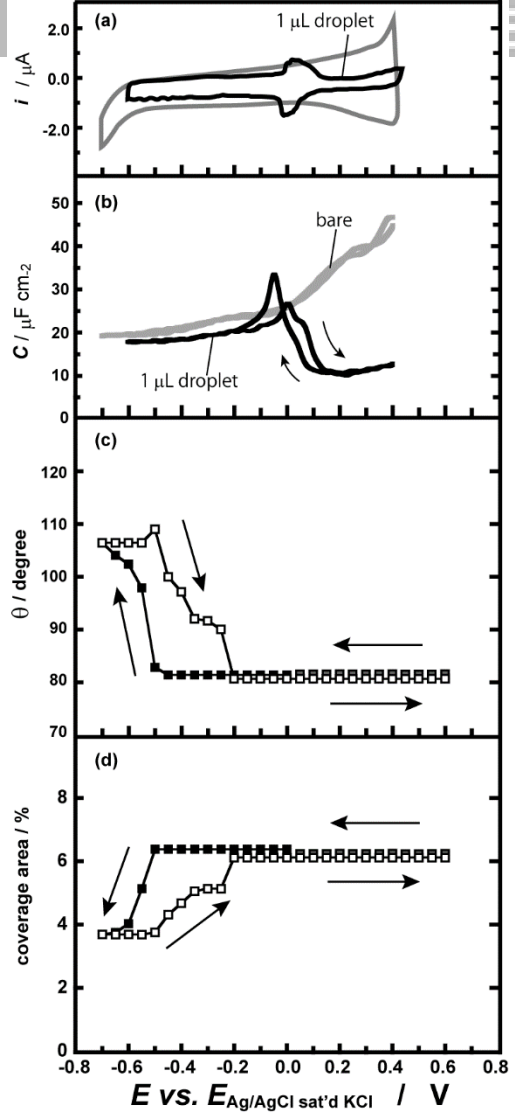

Figure 1

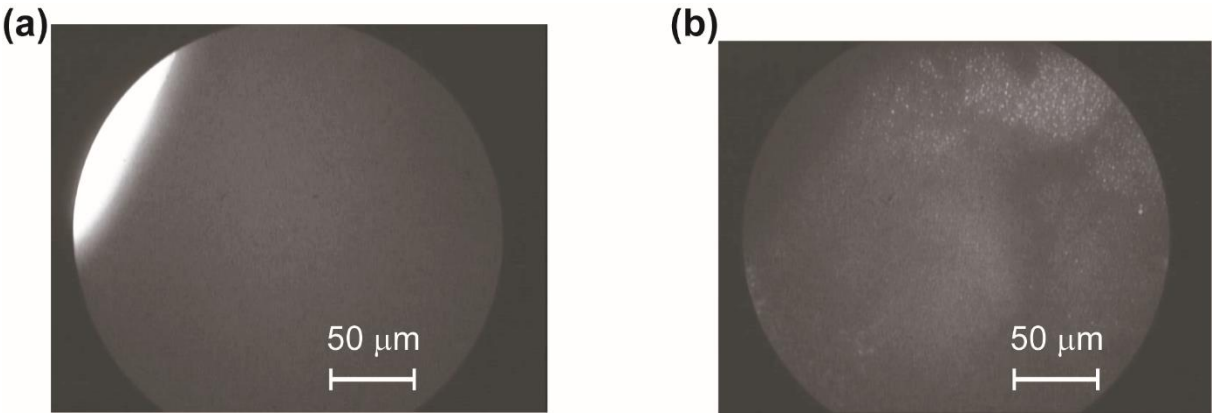

Figure 2

Figure 3

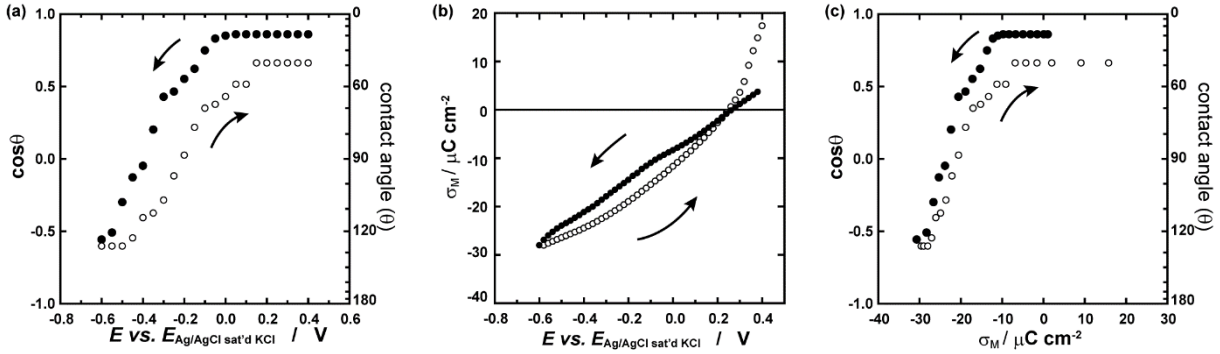

Figure 4

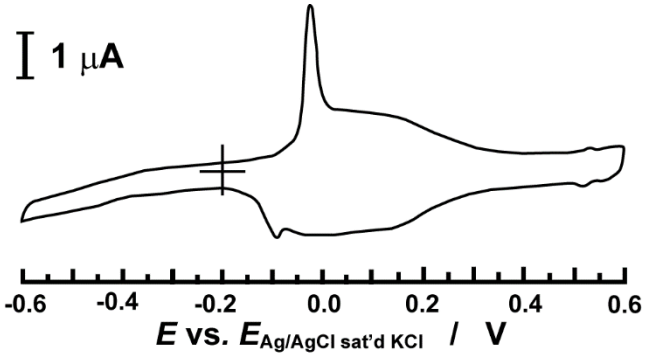

Figure 5

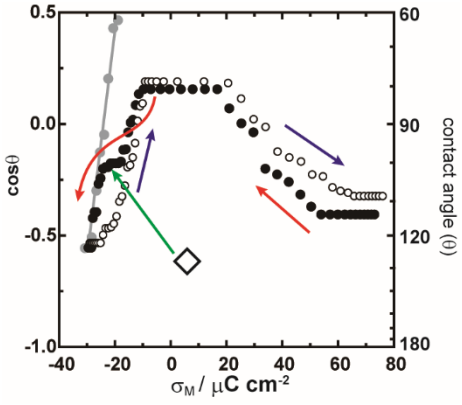

Figure 6

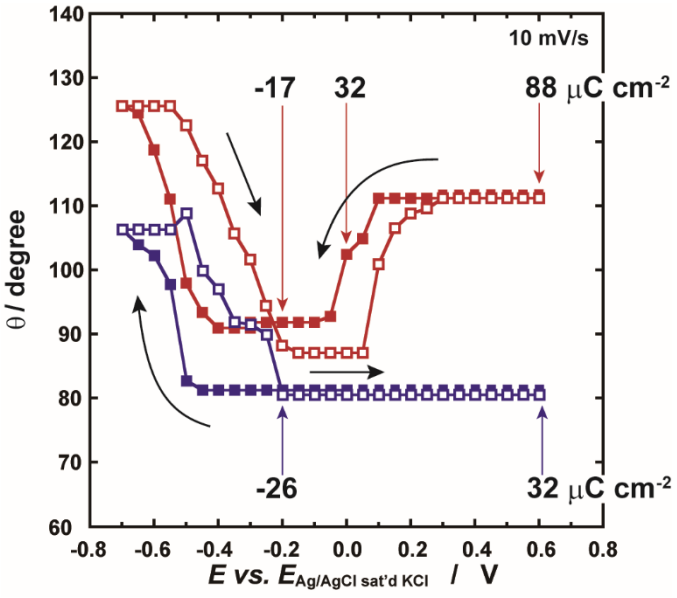

Figure 7